Analyst

PAPER

View Article Online
View Journal | View Issue

Cite this: *Analyst*, 2015, **140**, 7678

Monodispersity of magnetic immuno-nanoprobes enhances the detection sensitivity of low abundance biomarkers in one drop of serum†

Rey Y. Capangpangan,‡[a,b,c] Mira Anne C. dela Rosa,‡[d,e] Rofeamor P. Obena,[f] Yu-Jen Chou,[g] Der-Lii Tzou,[f] Shao-Ju Shih,[g] Ming-Hsi Chiang,[f] Chun-Cheng Lin*[a] and Yu-Ju Chen*[d,f]

To enhance the detection sensitivity of target clinical protein biomarkers, a simple and rapid nanoprobe-based immuno-affinity mass spectrometry assay employing biocompatible monodisperse magnetic nanoparticles (MNPs) is reported herein. The MNPs were synthesized *via* a streamlined protocol that includes (a) fabrication of core MNPs using the thermal decomposition method to minimize aggregation, (b) surface protection by gold coating (MNP@Au) and surfactant coating using MNP@IGEPAL to improve hydrophilicity, and lastly, (c) oriented functionalization of antibodies to maximize immuno-affinity. The enrichment performances of the monodisperse MNPs for the C-reactive protein (CRP) serum biomarker were then evaluated and compared with aggregated magnetic nanoparticles synthesized from the conventional co-precipitation method (MNP_{CP}). The detection sensitivity for CRP at an extremely low amount of serum sample (1 μL) was enhanced ~19- and ~15-fold when monodisperse MNP@Au and MNP@IGEPAL, respectively, were used. Furthermore, the detection sensitivity of CRP by this approach (1 ng mL^{-1}, S/N = 3) provided a 1000-fold sensitivity enhancement to the clinical cut-off (1 μg mL^{-1}) of CRP. We supposed that these observed improvements are due to the enhanced nanoparticle dispersibility and size uniformity which eliminated completely other non-specific binding of high-abundance serum proteins. Most interestingly, the enrichment efficiency correlates more closely with the MNP dispersibility than the ligand density. Our investigation revealed the critical role of MNP dispersibility, as well as provided mechanistic insight into its impact on immunoaffinity enrichment and detection of CRP in one drop of serum sample. This strategy offers an essential advantage over the other methods by providing a simple and facile biofunctionalization protocol while maintaining excellent solvent dispersibility of MNPs.

Received 28th July 2015,
Accepted 21st September 2015

DOI: 10.1039/c5an01530h

www.rsc.org/analyst

1. Introduction

The detection of proteins from human blood, serum or plasma relies primarily on immunoassays, such as enzyme-linked immunosorbent assay (ELISA). Despite its excellent detection sensitivity, this method requires delicate methodology development, especially good quality antibodies with high specificity to avoid false positive and negative results.[1] For clinical application, alternative methods possessing high sensitivity and reliability are under intense exploration. In recent years, magnetic nanoparticles (MNPs) have been actively explored for various biological applications, including bioseparation[2–4] and medical diagnostics[5] due to their remarkable properties such as superparamagnetism, biocompatibility and versatile surface functionality. By further surface functionalization with an affinity ligand or an antibody, isolation of biomolecules followed by various detection systems can be performed with various degrees of specificity and sensitivity. Though the fabrication methods of

[a]*Department of Chemistry, National Tsing Hua University, Hsinchu, Taiwan. E-mail: cclin66@mx.nthu.edu.tw*
[b]*Molecular Science and Technology, Taiwan International Graduate Program, Academia Sinica and Department of Chemistry, National Tsing Hua University, Taiwan*
[c]*Caraga State University, Butuan City, Philippines*
[d]*Department of Chemistry, National Taiwan University, Taipei, Taiwan. E-mail: yujuchen@gate.sinica.edu.tw*
[e]*Nano Science and Technology Program, Taiwan International Graduate Program, Academia Sinica and Department of Chemistry, National Taiwan University, Taiwan*
[f]*Institute of Chemistry, Academia Sinica, Taipei, Taiwan*
[g]*Department of Material Science and Engineering, National Taiwan University of Science and Technology, Taipei, Taiwan*

†Electronic supplementary information (ESI) available: Detailed experimental protocols, nanoprobe characterization and other supporting data. See DOI: 10.1039/c5an01530h

‡These authors contributed equally to this work.

MNPs are well-established, their successful application is highly dependent on the nanoparticle stability in a wide range of different conditions,[6,7] such as pH, temperature and ionic strength of different media.[7,8] Highly uniform magnetic nanoparticles, both in size and shape, compatible with biofluids are desirable to ensure reproducibility and high-quality performance.[9] Furthermore, to take full advantage of MNPs for biological applications, a stable MNP surface that can be easily functionalized with a wide range of ligand molecules and exhibit good solvent compatibility is another important pre-requisite.

For fabrication of ligand-conjugated MNPs, the nanoparticle aggregation presents a problematic issue influencing size and reactivity of nanostructured materials. Formation of nanoparticle aggregates likely reduces the surface area-to-volume ratio and the available reactive surface area, hence affecting the nanoparticle interfacial reactivity in suspension.[10] Due to large surface energy, magnetic nanoparticles tend to undergo uncontrolled aggregation,[4] which is particularly notable in iron oxide nanoparticles. Further aggregation occurs when the attractive magnetic forces are greater than the electrostatic repulsive forces between nanoparticles.[11] Such an aggregation tendency presents a challenge to their performance in target-specific extraction and detection. Bioseparation assays are highly dependent on magnetic nanoparticle homogeneity, size uniformity and excellent solvent dispersibility.[4,12] Once the particles are irreversibly aggregated, they lose important nanoscale features, such as their large surface-to-volume ratio necessary for high-density ligand conjugation and their ability to intimately interact with the target biological analytes.[13,14] MNP aggregation can also reduce the available nanoparticle surface area for protein binding, and induce protein conformational changes[15] which affect the ligand's binding specificity. Therefore, selective binding of aggregated nanoparticles to the target analytes becomes more challenging[16] due to induced serious non-specific adsorption of undesirable molecules present in the sample.

Over the past few decades, unprecedented developments in architecting MNPs with size-controlled and tailored physical properties have been reported. An appropriate choice of synthetic protocol is important to determine the particle size/shape, size uniformity as well as the nanoparticle surface chemistry.[17] To date, the thermal decomposition method has been reported to produce MNPs with a high level of stability and monodispersity.[18] While this technique has been proven to produce MNPs with a narrow size distribution, the resulting nanoparticles are generally dispersible in nonpolar solvents only,[19] which is not compatible with the hydrophilic biological environment. Hence, in order to implement MNPs for biological applications, strategies for surface functionalization with hydrophilic coatings as well as affinity ligands on these monodisperse nanoparticles to facilitate biomolecular recognition remains to be further explored. Furthermore, effective surface protection with appropriate stabilizers is imperative to maintain the MNP stability after synthesis. Biocompatible monodisperse gold-coated magnetic nanoparticles have been reported[20] with application to a few biological systems, including surface-enhanced Raman spectroscopy (SERS)-based magnetic bioassay for protein A,[21] and interactions with thiolated DNA.[22] By the use of a non-ionic surfactant (polyoxyethylene (5) nonylphenylether, branched), IGEPAL-encapsulated MNPs (IGEPAL CO-520) have been reported for DNA separation[23] and antitumor nanovehicle.[24] Despite the success of these protocols to fabricate monodisperse MNPs in selected systems, in-depth evaluation of the influence of the MNP properties on their analytical performance in detection sensitivity and specificity has not been reported.

In this work, we present a streamlined protocol for biocompatible monodisperse magnetic nanoparticles with excellent solvent dispersibility to enhance the sensitivity for biomarker detection in a low amount of serum sample. Specifically, we report two surface functionalization strategies: gold-coated magnetic nanoparticles (MNP@Au) and IGEPAL-coated magnetic nanoparticles (MNP@IGEPAL) based on monodisperse MNPs were synthesized by the thermal decomposition method[18] to fabricate biocompatible well-dispersed MNPs for highly specific extraction and detection of protein biomarkers. Using an inflammatory and cardiovascular biomarker C-reactive protein (CRP) as the proof-of-concept system, we observed the impact of nanoparticle dispersibility and size uniformity to enhance the sensitivity and specificity of magnetic bioseparation and detection of CRP in serum, which presents the most complex biofluid composed of thousands of proteins with a wide dynamic range (10^9).[25] To the best of our knowledge, this is the first attempt to provide correlation between the nanoparticle physical properties, including polydispersity index (PDI), dispersion coefficient and characteristic decay time and its capability of biomolecular affinity-based extraction.

2. Experimental

2.1 Streamlined protocol for immuno-MNP synthesis

The detailed synthetic protocols of various MNPs are presented in the ESI 1.1 to 1.6† (Fig. S1 and S2†). In brief, gold-coated magnetic nanoparticles (MNP@Au) were synthesized based on a modified protocol[22,26] followed by amine functionalization.[27] Similarly, amine-modified nanoparticles using the IGEPAL CO-520 surfactant (polyoxyethylene (5) nonylphenylether, branched, MNP@IGEPAL) were prepared by adopting the reported protocol with some modifications.[28] Fabrication of conventional core magnetic nanoparticles was carried out *via* the co-precipitation method using $FeCl_2$ and $FeCl_3$ under basic conditions and subsequent amine functionalization was carried out as described from our previous report.[29–31] Lastly, antibodies were immobilized to the nanoparticle surface following the procedure of Lin *et al.*[29] The amount of protein conjugated in the nanoparticle was measured using a Bicinchoninic acid (BCA) protein assay kit (Pierce™) (ESI 1.7†). Size and morphology characterization and confirmation of surface functionalization of the MNPs are detailed in the ESI 1.8† (Fig. S3–S5†).

2.2 Aggregation and sedimentation experiment

Aggregation and sedimentation experiments were carried out following the published protocol with some modifications

(ESI 1.9†).[32,33] Sedimentation experiments were carried out in PBS buffer (pH 7.4) and PBS-diluted serum using concentrations that mimic the protein enrichment conditions. The optical absorbance at 508 nm as a function of time was monitored using a UV-Vis spectrophotometer (8453 UV-Vis, Agilent Technologies). Sedimentation curves were obtained by plotting the normalized absorbance *versus* time. The decay time was determined by fitting the curve using the exponential decay function by OriginLab® (V.8) software. Likewise, the hydrodynamic radius was obtained from the Dynamic Light Scattering (DLS) experiment (Malvern Zetasizer Nano ZS). All measurements were carried out at room temperature.

2.3 Immunoaffinity extraction

Boronic acid-oriented antibody nanoprobes (2 μL, 10 mg mL^{-1}) were added to a standard protein solution in phosphate buffered saline (PBS, pH ~ 7.4, ionic strength = 0.1675 M, 2–1000 ng mL^{-1}) or human serum (20 μL). The solution was incubated at room temperature for 1 hour in a rotary mixer (gentle mixing to avoid disruption of the nanoparticle–antigen complex). After extraction, the MNPs were separated using a magnet, washed twice with Tween-TBS (TTBS, 200 μL) and then twice with deionized water (200 μL).

2.4 MALDI-TOF analysis

The MNPs were reconstituted in deionized water (1 μL) and sinapinic acid (SA, 1 μL, 7.5 mg mL^{-1} in 0.1% TFA/50% ACN solution), and directly transferred onto a MALDI plate. All MALDI spectra were obtained on an Applied Biosystems 4800 MALDI-TOF (Applied Biosystems, Foster City, CA) equipped with an Nd/YAG laser (355 nm). A typical spectrum was obtained by averaging 3000 laser shots from 20 positions within the sample well, followed by baseline correction and Gaussian smoothing using Data Explorer software (Applied Biosystems).

3. Results and discussion

3.1 Biocompatible monodisperse nanoprobes

As shown in Fig. 1, when the nanoparticle forms large aggregates (as in the case of nanoparticles derived from the co-precipitation method, Fig. 1b), their surface-to-volume ratio will be reduced which affects their interaction with the target protein.[14] In contrast, we surmise that optimum coverage of ligands could be attained for well-dispersed nanoparticles (Fig. 1a), which would increase their enrichment efficiency and

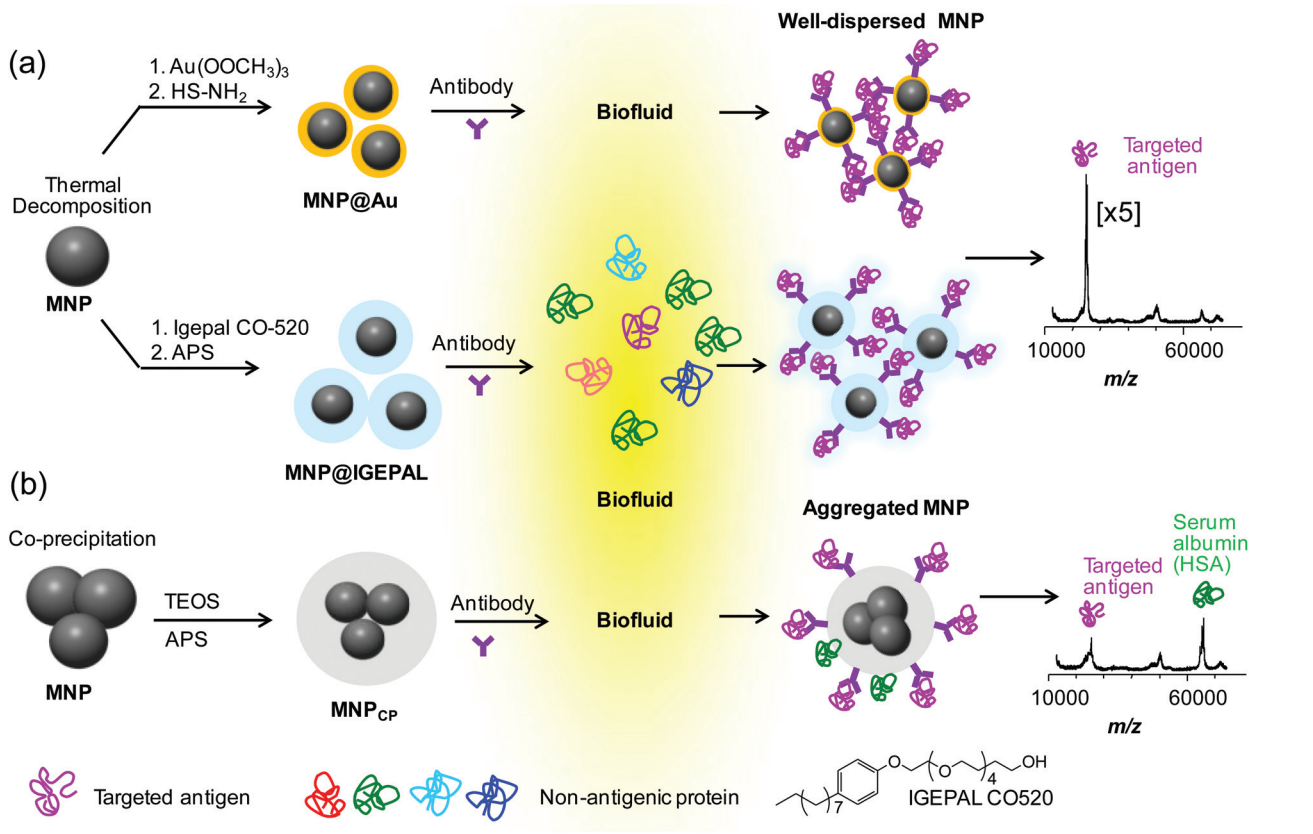

Fig. 1 (a) Sensitivity and specificity enhancement with well-dispersed magnetic immuno-nanoparticles derived from the thermal decomposition method, subsequent gold or surfactant coating MNPs and antibody conjugation; (b) magnetic nanoprobes derived from the co-precipitation method, subsequent silica coating and antibody conjugation. After enrichment of target antigen in biofluid, MALDI mass spectrometry analysis shows sensitivity and specificity enhancement by well-dispersed MNPs compared to aggregated MNPs.

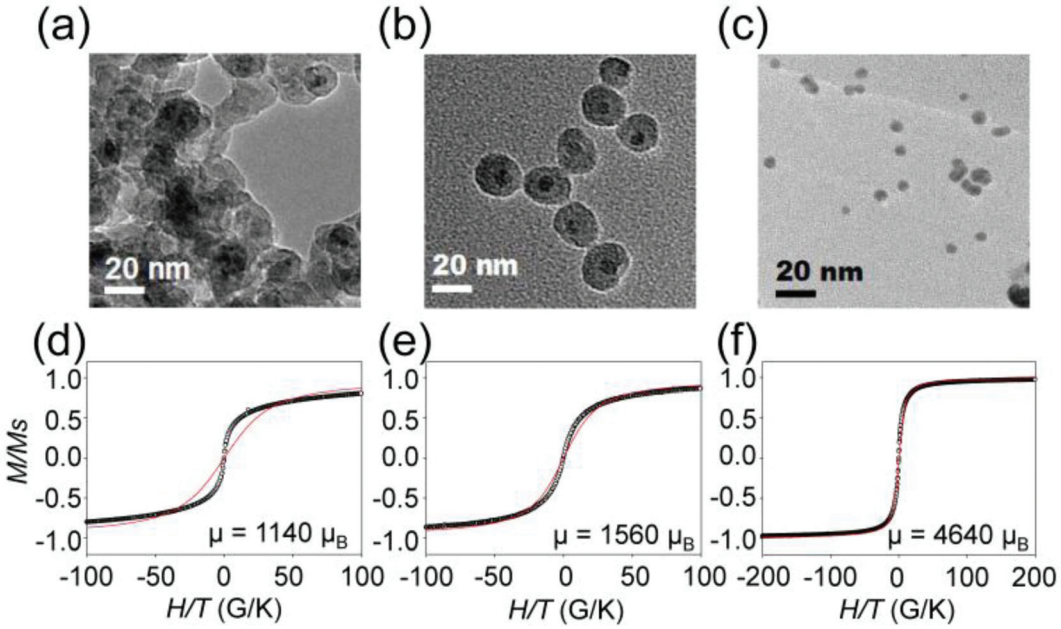

Fig. 2 Transmission electron microscopy (TEM) images of (a) MNP_{CP}, (b) MNP@IGEPAL and (c) MNP@Au; and the normalized magnetization curves as a function of *H*/*T* at 300 K for samples (d) MNP_{CP}, (e) MNP@IGEPAL and (f) MNP@Au. The experimental data are displayed in circles (black) and the solid line (red) represents the best fit to the theoretical expression based on the Langevin equation.

detection sensitivity. Moreover, we suppose that the large nanoparticle aggregates (non-uniform sizes) would have a large hydrodynamic diameter and more exposed unfunctionalized surfaces, which can induce serious non-specific binding of unwanted biomolecules,[34] hence, influence the enrichment efficiency of the nanoprobe.

To prove our hypotheses stated above, the nanoprobes were prepared at three levels: (1) synthesis of the core nanoparticle by the thermal decomposition method, (2) surface protection by employing inorganic and surfactant coating, and (3) oriented antibody immobilization to enhance immunoactivity. At the first level, the thermal decomposition method was employed to synthesize monodisperse core magnetic nanoparticles.[18] At the second level, two different coating approaches for the pre-synthesized magnetic nanoparticles were adapted: (1) inorganic metal shell coating using gold (MNP@Au), and (2) surfactant encapsulation using IGEPAL CO-520 (MNP@IGEPAL). Then, at the third level, amine functionality was subsequently anchored on the surface of the nanoparticles for direct functionalization with different antibodies (or ligands) against the target analyte. The MNP@Au was functionalized with amine by ligand exchange using cysteamine to produce NH_2-MNP@Au, while the MNP@IGEPAL was reacted with aminopropylsilane (APS) to produce NH_2-MNP@IGEPAL. For comparison purposes, amine-functionalized magnetic nanoparticles derived from the chemical co-precipitation (MNP_{CP}) method was prepared by direct silica and APS coating (NH_2-MNP_{CP}).[29] The synthesized nanoparticles were then characterized by IR spectroscopy, Energy Dispersive X-ray Spectroscopy (EDX) and X-ray Photoelectron Spectroscopy (XPS) to confirm the functionalization process (Fig. S3–S5,† respectively).

As shown in the TEM images, the synthesized amine-functionalized magnetic nanoparticles have narrow size distributions (uniform size) and are non-aggregated with an average size of 7.75 ± 0.791 nm (CV = 10.2%) and 22.38 ± 1.245 nm (CV = 5.56%) for NH_2-MNP@Au (Fig. 2c) and NH_2-MNP@IGEPAL (Fig. 2b; note: the core MNP is the dark spot at the center surrounded by the surfactant and silica shell in lighter grayish hue), respectively. By definition, monodisperse nanoparticles are defined as those with less than 5% coefficient of variation (CV) and near-monodisperse as those with less than 15%.[35] According to this criterion, both NH_2-MNP@Au and NH_2-MNP@IGEPAL appear to be near-monodisperse. Conversely, severe aggregation was observed for NH_2-MNP_{CP} (Fig. 2a), and hence the size distribution of the nanoparticle cannot be ascertained. A high magnetic moment of MNP is essential for efficient isolation and recovery of the antigen–antibody–nanoparticle complex from the solution. The magnetic properties of the amine-modified nanoparticles were also measured (Fig. 2). The results suggest that the three magnetic nanoparticles have good magnetic properties. Of the three, NH_2-MNP@Au has the highest effective magnetic moment ($4640\mu_B$), indicating Au coating has an insignificant influence on reducing the magnetic susceptibility of MNPs. On the other hand, NH_2-MNP_{CP} has the lowest effective magnetic moment ($1140\mu_B$), revealing that the silica shell coating somehow influences the magnetic properties of MNP_{CP}. Such reduced magnetization is likely attributed to the decreased dipole–dipole interactions of the particles and lower exchange of coupling energy in the

presence of a nonmagnetic polymer layer on the MNP surface.[36]

3.2 Immunoaffinity enrichment and detection of C-reactive protein (CRP)

Next, we fabricated nanoprobes for immunoaffinity enrichment of proteins by conjugating antibodies on the nanoparticles. For this purpose, we chose the C-reactive protein (CRP, mass = 23 026 Da, Calbiochem) as our model target analyte. The C-reactive protein (CRP) is reported to be a good and sensitive diagnostic biomarker for the inflammatory process and cardiovascular diseases.[37] For most infections and inflammations, the concentration of CRP can rise above 100 μg mL^{-1} (from a normal level of <5 μg mL^{-1}). CRP concentrations can be categorized as low, average and high risk of developing cardiovascular diseases when the CRP level is in the range of <1 μg mL^{-1}, 1.0–3.0 μg mL^{-1} and >3.0 μg mL^{-1}, respectively. To optimize the immuno-activity of the antibody, self-oriented immobilization of antibodies on each magnetic nanoparticle was achieved by covalent conjugation through the carbohydrate moiety within the constant domain, Fc, of the antibody.[29] The amount of antibody conjugated to the nanoparticles was quantified using the bicinchoninic acid assay (BCA assay). The amounts of the anti-CRP antibody conjugated to MNPs are 15.3 μg, 7.7 μg and 18.4 μg per mg of MNP@Au, MNP@IGEPAL and MNP_{CP}, respectively. The antibody-conjugated nanoparticles were incubated with standard protein solution or human serum for 1 hour. The protein–antibody–nanoparticle complex was isolated using a magnet, and analyzed directly by matrix-assisted laser desorption/ionization mass spectrometry (MALDI-TOF MS).

Fig. 3 shows the comparison of the MALDI spectra of CRP enriched from PBS (100 ng mL^{-1} and 5 ng mL^{-1}) by the three nanoprobes. As shown, at high analyte concentration (100 ng mL^{-1}), all the nanoprobes were able to enrich the target analyte with an excellent S/N ratio (Fig. 3a–c). Furthermore, Fig. 3d–f show that all the newly fabricated nanoprobes can enrich CRP as low as 5 ng mL^{-1} but with different enrichment recoveries. Based on the peak area, the MNP@Au exhibited 9- and 6-fold performance (peak area = 60 873, S/N = 28.7) superior to either MNP@IGEPAL (peak area = 6687, S/N = 6.6) or MNP_{CP} (peak area = 10 884, S/N = 9.8), respectively. With the criterion of S/N = 3, the LOD is 1 ng ml^{-1}. The results demonstrated that our approach is 120 times more sensitive than the previously reported magnetic immunoassay (0.12 μg mL^{-1}) for CRP and dramatically enhanced the detection sensitivity of the CRP clinical cut-off in the serum sample (1 μg mL^{-1}) by 1000-fold.[38] A comparison with the analytical performance of different magnetic immuno-assays for CRP detection is tabulated in ESI 1.11.† This implies the promising utility of monodisperse MNP@Au for clinical diagnosis of low-abundant biomarkers, which requires detection sensitivities down to low concentration (ng mL^{-1}) ranges for clinical serum biomarkers.[39]

While PBS buffer is a good starting point to evaluate the enrichment efficiency, for real diagnostic applications,

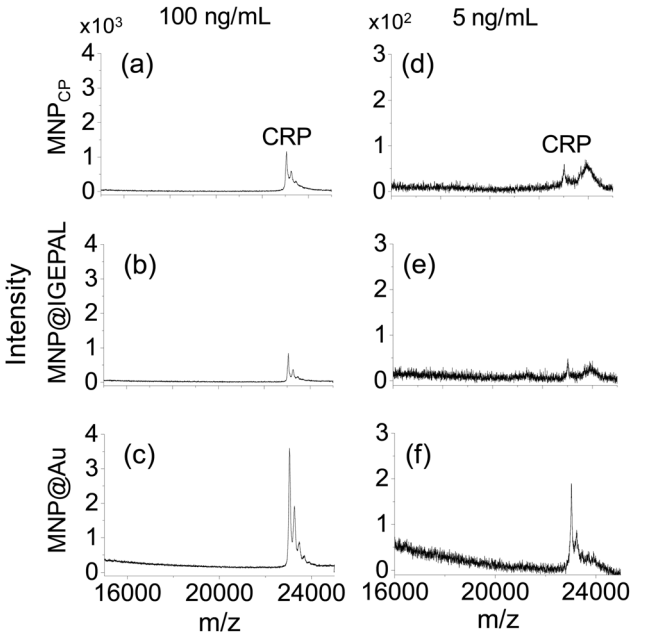

Fig. 3 Sensitive detection of biomarker candidates by well-dispersed nanoprobes: MALDI spectra of CRP (100 ng mL^{-1}) enriched from PBS buffer by (a) MNP_{CP}; (b) MNP@IGEPAL; (c) MNP@Au. MALDI spectra of CRP (5 ng mL^{-1}) enriched from PBS buffer by (d) MNP_{CP}; (e) MNP@IGEPAL; (f) MNP@Au.

however, the biomarkers are usually extracted from complex samples such as tissue or body fluids. Although human serum or plasma is the preferred clinical specimen due to its non-invasive nature of collection, yet serum proteome has a wide protein concentration range spanning nine orders of magnitude[25] and such complexity greatly affects the enrichment efficiency for target proteins. To demonstrate the biocompatibility of the nanoparticles in human serum, CRP was isolated from the serum of a healthy individual (the CRP concentration is estimated to be between 0.8 and 3 μg mL^{-1}).[40] The most dramatic effect by the use of different MNPs was observed in the extraction of CRP from a minute amount of serum. In only 1 μL serum (approximately 1/30 volume of one drop of blood), CRP was enriched by both the well-dispersed MNP@Au and MNP@IGEPAL (Fig. 4e and f), but barely observed by the aggregated MNP_{CP} (Fig. 4d). This is equivalent to a ~19- and ~15-fold enhancement of MNP@Au and MNP@IGEPAL over MNP_{CP} (Fig. 4h). With a higher amount of available serum (10 μL), the MNP@Au and MNP@IGEPAL also demonstrated superior performance (Fig. 4a–c) with 8-fold and 6-fold signal enhancement, respectively, compared to that of MNP_{CP} (Fig. 4g). Considering that the concentration of CRP in the serum of healthy individuals is between 0.8 and 3 μg mL^{-1},[40] the results show that both MNP@Au and MNP@IGEPAL are highly efficient to isolate sub-nanogram levels of protein from a very complex mixture like serum.

Non-specific binding of abundant proteins, such as serum albumin (55% in serum),[41] is a commonly encountered chal-

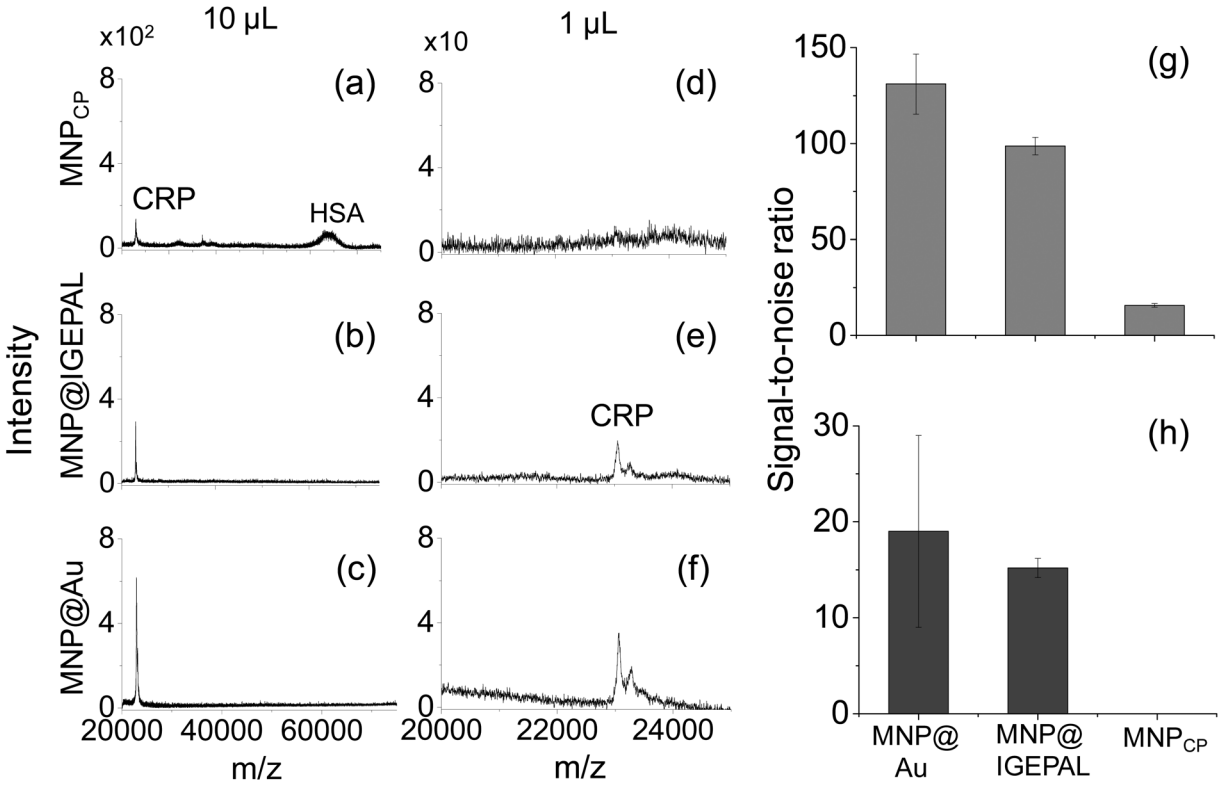

Fig. 4 Enrichment of endogenous CRP from 10 μL diluted serum from a healthy individual is shown in (a) MNP_{CP}; (b) MNP@IGEPAL; and (c) MNP@Au. MALDI spectra of CRP from 1 μL serum (about 1/30 of "one-drop" of blood) enriched using (d) MNP_{CP}; (e) MNP@IGEPAL; and (f) MNP@Au. Comparison of signal-to-noise ratios of CRP enriched from (g) 10 μL diluted serum and (h) 1 μL diluted serum.

lenge that causes false-positive biomarker detection.[30] In our case, the well-dispersed nanoprobes also demonstrated specificity for protein extraction. In a high mass range (Fig. 4a–c), no signal of non-specific binding from serum albumin (mass: 66 kDa) was observed by the use of the MNP@Au and MNP@IGEPAL, while traces of serum albumin were observed in the MALDI spectra with the use of MNP_{CP} (Fig. 4a). The sensitivity enhancement in serum can be attributed to reduced non-specific binding exhibited by the MNP@Au and MNP@IGEPAL nanoprobes. Although the performances of MNP@IGEPAL and MNP_{CP} were comparable in PBS buffer, MNP_{CP} has a relatively poor performance in serum. This can be attributed to the non-specific binding of undesirable biomolecules on the nanoparticle, thus lowering its enrichment capacity and efficiency.[42]

In clinical diagnosis, enzyme-linked immunosorbent assay (ELISA) has been used for CRP detection. The elimination of non-specific binding is a significant advantage over the commonly used ELISA, which is susceptible to matrix interference that causes false-positive or false-negative results.[1] In addition to its sufficient sensitivity, the nanoprobe-based mass spectrometry method provides unambiguous detection of serum biomarkers without the need for a highly specific antibody, which is one of the limitations of the ELISA method.

3.3 Enrichment sensitivity and specificity correlated with nanoparticle dispersibility and size uniformity

Inspired by these results, we examined the possible factors, including nanoprobe dispersibility, surface coating and size uniformity, which may have influenced the enrichment efficiency of the nanoprobes. We suppose that if the nanoprobe is well-dispersed in the reaction buffer, then it has more time to intimately interact with the analyte before settling down, thus, yielding a better enrichment performance. Additionally, surface coating will also influence nanoparticle stability and in turn, its dispersibility; whereas magnetic susceptibility will influence the enrichment recovery of the nanoprobes. Likewise, size uniformity may also have an impact on the surface ligand conjugation density as well as surface protection to minimize non-specific interactions with the undesirable molecules, which is critical to the sensitivity and specificity of the probes. When the nanoparticles are incubated in the biofluids (*e.g.* plasma), highly abundant proteins will initially bind to the surface of the nanoparticles.[43] In some cases, the adsorption of biological molecules can cause the nanoparticle colloids to destabilize and aggregate,[44] which trap the abundant proteins. Thus, it is crucial to maintain nanoparticle stability (or avoiding aggregation) for efficient and selective bioseparation. Since the crystalline state does not accurately reflect the degree of nanoparticle aggregation in

Table 1 Summary of nanoparticle physicochemical properties

NH_2-MNP	TEM size (nm)	DLS diameter[a] (nm)	PDI value	Magnetic moment	Decay time (τ, s)		Dispersion coefficient (D, $m^2\ s^{-1}$, $\times 10^{-11}$)	
					PBS	Serum	PBS	Serum
MNP@Au	7.46 ± 1.47	18.17	0.09	4640	4095	6590	2.40	0.172
MNP@IGEPAL	25.5 ± 2.0	295.3	0.2	1560	3195	4506	0.148	0.106
MNP_{CP}	N.D.	396.1	0.5	1140	708	570	0.110	0.0787

[a] Measured using the Dynamic Light Scattering (DLS) experiment.

solution,[45] the aggregation behavior of the nanoparticles in the dispersing buffer could not be characterized by TEM alone. To evaluate the dispersibility of these nanoparticles, the polydispersity indices (PDI) from the dynamic light scattering (DLS) experiment were measured. A low PDI value indicates that nanoparticles are monodisperse in a given medium.[46] The dynamics of the aggregation process and the suspension stability in the dispersing buffer were shown by the decay time profiles of each of the nanoprobes. Aggregation dynamics can be assessed in terms of the characteristic decay time (τ)[32] by plotting the normalized UV absorbance (A/A_0) of the nanoparticle suspension (PBS-diluted serum, 0.2 mg mL^{-1} and in PBS, 0.02 mg mL^{-1}) *versus* time.

In theory, the behavior of the suspended particles in solution is best described by the Stokes–Einstein relationship (dispersion coefficient, $D = kT/6\pi\eta R_h$),[47] which describes the hydrodynamic interaction of the particles and their random movement (Brownian motion) in solution.[48] Due to its small size (7.46 nm, Table 1) and hydrodynamic diameter ($2R_h$, 18.17 nm, Table 1), NH_2-MNP@Au forms the most stable colloidal suspensions ($D_{PBS} = 2.4 \times 10^{-11}\ m^2\ s^{-1}$; $D_{ser} = 1.72 \times 10^{-12}\ m^2\ s^{-1}$) of the three MNPs and are monodisperse (PDI = 0.09). This result indicates that the likely greater Brownian movement may disfavor inter-particle hydrodynamic interactions and result in the MNPs being in suspension for a longer time (τ_{PBS} = 4095 s; τ_{ser} = 6590 s). On the other hand, the lowest dispersion coefficients of NH_2-MNP@IGEPAL ($D_{PBS} = 1.48 \times 10^{-12}\ m^2\ s^{-1}$; $D_{ser} = 1.06 \times 10^{-12}$) indicating a deviation from the Stokes–Einstein relationship suggest polydisperse-like behaviour in solution. In such a case, they may settle faster (τ_{PBS} = 3195 s; τ_{ser} = 4506 s) than when spatially disconnected. When the size is irresolute and the hydrodynamic diameter is huge (396.1 nm), such as in the case of NH_2-MNP_{CP}, polydispersibility (PDI = 0.5) and aggregation are inevitable. Thus, the nanoparticles cannot diffuse effectively in the medium ($D_{PBS} = 1.10 \times 10^{-12}\ m^2\ s^{-1}$; $D_{ser} = 7.87 \times 10^{-13}\ m^2\ s^{-1}$) and sediment very fast, as clearly shown in the shortest decay time (τ_{PBS} = 708 s; τ_{ser} = 570 s).

The decay curves of these three nanoprobes (Fig. 5) reveal the same trend as that of the PDI. In PBS buffer, NH_2-MNP@Au and NH_2-MNP@IGEPAL decay curves have ~6-fold and 5-fold longer decay time, respectively, than NH_2-MNP_{CP} (Fig. 5a). In diluted serum, a more dramatic result was observed: NH_2-MNP@Au and NH_2-MNP@IGEPAL showed ~12-fold and ~8-fold longer decay time than NH_2-MNP_{CP} (Fig. 5b). Hence, the dispersibility of MNPs expressed by the dispersion coefficient and the polydispersity index is inversely correlated with their sedimentation time. Such nanoparticle behavior indicates that serum proteins can prevent nanoparticle aggregation and sedimentation.[49] Through protein adsorption and the imparted net surface charge, soluble proteins can induce stability to nanoparticles in serum. Both the results for MNP@Au and MNP@IGEPAL agree with the published

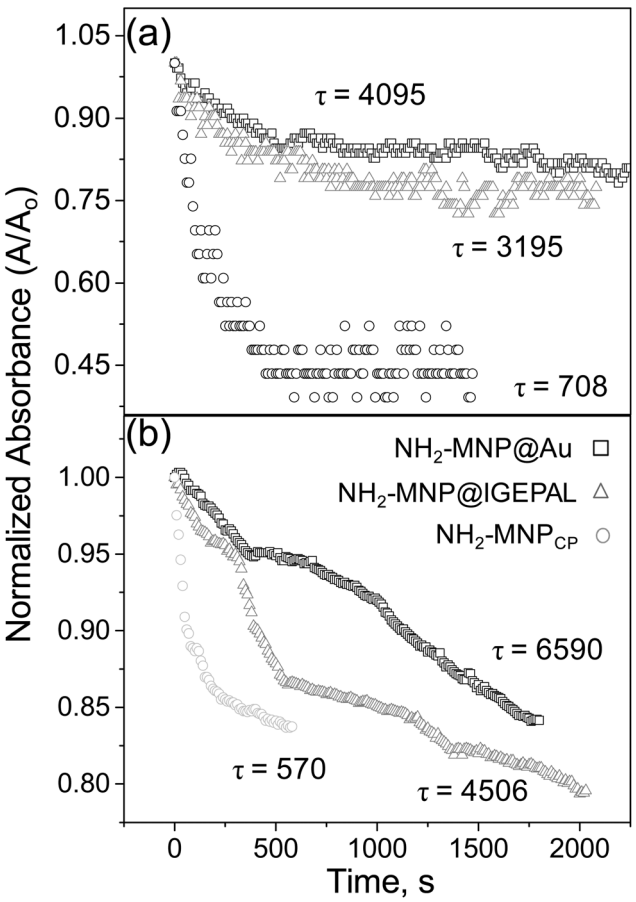

Fig. 5 Decay time profile of magnetic nanoparticles in (a) PBS buffer at 0.02 mg mL^{-1} concentration and (b) PBS-diluted serum.

report,[49] but not MNP_{CP}. The latter settled down faster in serum than in PBS buffer, which may be due to its different surface chemistry compared with the first two nanoprobes. Because of its diminished protein coating and reduced stability, MNP_{CP} could have aggregated and sedimented faster in serum than in PBS.

To gain more insight on the influence of nanoparticle dispersibility, the correlation between the antibody density, nanoprobe dispersibility and its enrichment efficiency in serum, expressed as the signal-to-noise ratio in the MALDI spectra, was evaluated. As shown in Fig. 4g and h the S/N was observed to proportionally increase with the decay time (Fig. 6a), showing the correlation between the nanoparticle enrichment efficiency and its dispersibility. At a constant amount of nanoparticles, *i.e.*, regardless of the antibody density, however, the antibody density on the nanoprobes has little or no correlation with the S/N ratios. Though the MNP_{CP} has the highest antibody density (18.4 μg Ab per mg) compared to MNP@Au (15.3 μg mg^{-1}) and MNP@IGEPAL (7.7 μg mg^{-1}) (Fig. 6b), MNP@Au gave the best enrichment performance. Interestingly, despite the low antibody density of MNP@IGEPAL, it also has 15-fold better efficiency than MNP_{CP}. Therefore, we conclude that the enrichment efficiency correlates more closely with the MNP dispersibility than the ligand density.

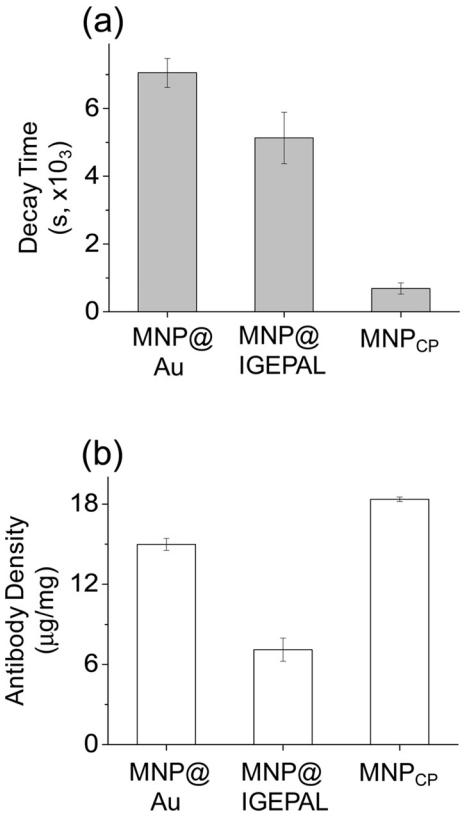

Fig. 6 (a) Decay time of the nanoparticles; (b) antibody density of antibody-conjugated nanoprobes.

4. Conclusion

In summary, by systematically designing a streamlined protocol based on thermal decomposition, and gold and surfactant coating, monodisperse immuno-MNPs, which are stable in PBS buffer and in serum, were fabricated. Among the monodisperse magnetic nanoparticles tested, MNP@Au has the most significant enhanced sensitivity in detecting CRP in both PBS buffer and human serum. The detection sensitivity of 1 ng mL^{-1} (S/N = 3) translated to a 120-fold enhancement compared to previous MNP-based immunoassays and is 1000-fold below the clinical cut-off of CRP for diagnosis.[38] More importantly, both MNP@Au and MNP@IGEPAL exhibited good sensitivity and specificity in one drop of serum with minimal non-specific adsorption by other interfering molecules. This highlights the advantage of the monodisperse nanoprobe-based enrichment over the conventional ELISA method, which is prone to interference from the highly complex human serum sample.

Among the physicochemical factors including dispersibility (affected by size, hydrodynamic diameter and viscosity of the medium), longer decay time (affected by medium dispersibility) and magnetic susceptibility (affected by coating), the efficiencies for immunoaffinity enrichment were found to closely correlate with the decay time of the nanoparticles. We have demonstrated that dispersibility greatly affects the enrichment of the C-reactive protein and performance of the nanoprobe-based mass spectrometry assay. The results may be attributed to the synergy between the dispersibility and size uniformity of the nanoparticles. The well-dispersed magnetic nanoparticles provide a stable suspension which increases the probability of affinity-based extraction of the target analyte, while the size uniformity provides better specificity of the nanoprobes to exclude non-specific extraction. With the demonstrated enhancement on enrichment sensitivity and specificity, we believe that the well-dispersed nanoprobes are promising materials not only for the detection and quantification of other disease biomarkers from clinical specimens by mass spectrometry, but also by other detection systems.

Acknowledgements

This work was fully supported by grants from Academia Sinica Research Project on Nanoscience and Technology and the Ministry of Science and Technology (MOST), Taiwan. The authors also would like to acknowledge the BCF Core Facility, Academia Sinica for the use of the Zetasizer nano ZS.

Notes and references

1 J. Tate and G. Ward, *Clin. Biochem. Rev.*, 2004, **25**, 105.
2 Y. Li, X. Zhang and C. Deng, *Chem. Soc. Rev.*, 2013, **42**, 8517–8539.

3 L. H. Reddy, J. L. Arias, J. Nicolas and P. Couvreur, *Chem. Rev.*, 2012, **112**, 5818–5878.
4 Y. Pan, X. Du, F. Zhao and B. Xu, *Chem. Soc. Rev.*, 2012, **41**, 2912–2942.
5 S. Mornet, S. Vasseur, F. Grasset and E. Duguet, *J. Mater. Chem.*, 2004, **14**, 2161–2175.
6 A. H. Lu, E. e. L. Salabas and F. Schüth, *Angew. Chem., Int. Ed.*, 2007, **46**, 1222–1244.
7 M. Pavlin and V. B. Bregar, *Dig. J. Nanomater. Bios.*, 2012, **7**, 1389–1400.
8 Y. Park, R. D. Whitaker, R. J. Nap, J. L. Paulsen, V. Mathiyazhagan, L. H. Doerrer, Y. Q. Song, M. D. Hurlimann, I. Szleifer and J. Y. Wong, *Langmuir*, 2012, **28**, 6246–6255.
9 B. Bhushan, D. Luo, S. R. Schricker, W. Sigmund and S. Zauscher, *Handbook of Nanomaterials Properties*, Springer Science & Business Media, 2014.
10 B. Issa, I. M. Obaidat, B. A. Albiss and Y. Haik, *Int. J. Mol. Sci.*, 2013, **14**, 21266–21305.
11 D. Rosická and J. Šembera, *Nanoscale Res. Lett.*, 2013, **8**, 1–9.
12 M. Colombo, S. Carregal-Romero, M. F. Casula, L. Gutierrez, M. P. Morales, I. B. Bohm, J. T. Heverhagen, D. Prosperi and W. J. Parak, *Chem. Soc. Rev.*, 2012, **41**, 4306–4334.
13 J. F. Berret, N. Schonbeck, F. Gazeau, D. E. Kharrat, O. Sandre, A. Vacher and M. Airiau, *J. Am. Chem. Soc.*, 2006, **128**, 1755–1761.
14 Q. A. Pankhurst, J. Connolly, S. K. Jones and J. Dobson, *J. Phys. D: Appl. Phys.*, 2003, **36**, R167–R181.
15 S. R. Saptarshi, A. Duchi and A. L. Lopata, *J. Nanobiotechnol.*, 2013, **11**, 1–12.
16 D. Li and R. B. Kaner, *J. Am. Chem. Soc.*, 2006, **128**, 968–975.
17 P. Tartaj, M. d. P. Morales, S. Veintemillas-Verdaguer, T. González-Carreño and C. J. Serna, *J. Phys. D: Appl. Phys.*, 2003, **36**, R182–R197.
18 S. Sun, H. Zeng, D. B. Robinson, S. Raoux, P. M. Rice, S. X. Wang and G. Li, *J. Am. Chem. Soc.*, 2004, **126**, 273–279.
19 C. Ravikumar and R. Bandyopadhyaya, *J. Phys. Chem. C*, 2011, **115**, 1380–1387.
20 L. Wang, H.-Y. Park, S. I.-I. Lim, M. J. Schadt, D. Mott, J. Luo, X. Wang and C.-J. Zhong, *J. Mater. Chem.*, 2008, **18**, 2629–2635.
21 H.-Y. Park, M. J. Schadt, L. Wang, I.-I. S. Lim, P. N. Njoki, S. H. Kim, M.-Y. Jang, J. Luo and C.-J. Zhong, *Langmuir*, 2007, **23**, 9050–9056.
22 I. Robinson, D. Tung le, S. Maenosono, C. Walti and N. T. Thanh, *Nanoscale*, 2010, **2**, 2624–2630.
23 K. Kang, J. Choi, J. H. Nam, S. C. Lee, K. J. Kim, S.-W. Lee and J. H. Chang, *J. Phys. Chem. B*, 2008, **113**, 536–543.
24 H. Li, Z. Li, J. Zhao, B. Tang, Y. Chen, Y. Hu, Z. He and Y. Wang, *Nanoscale Res. Lett.*, 2014, **9**, 146.
25 R. Pieper, C. L. Gatlin, A. J. Makusky, P. S. Russo, C. R. Schatz, S. S. Miller, Q. Su, A. M. McGrath, M. A. Estock, P. P. Parmar, M. Zhao, S.-T. Huang, J. Zhou, F. Wang, R. Esquer-Blasco, N. L. Anderson, J. Taylor and S. Steiner, *Proteomics*, 2003, **3**, 1345–1364.
26 L. Wang, J. Luo, Q. Fan, M. Suzuki, I. S. Suzuki, M. H. Engelhard, Y. Lin, N. Kim, J. Q. Wang and C. J. Zhong, *J. Phys. Chem. B*, 2005, **109**, 21593–21601.
27 C. S. S. R. Kumar and F. Mohammad, *J. Phys. Chem. Lett.*, 2010, **1**, 3141–3146.
28 M. Zhang, B. L. Cushing and C. J. O'Connor, *Nanotechnology*, 2008, **19**, 085601.
29 P. C. Lin, S. H. Chen, K. Y. Wang, M. L. Chen, A. K. Adak, J. R. Hwu, Y. J. Chen and C. C. Lin, *Anal. Chem.*, 2009, **81**, 8774–8782.
30 P. C. Lin, P. H. Chou, S. H. Chen, H. K. Liao, K. Y. Wang, Y. J. Chen and C. C. Lin, *Small*, 2006, **2**, 485–489.
31 K. Y. Wang, S. A. Chuang, P. C. Lin, L. S. Huang, S. H. Chen, S. Ouarda, W. H. Pan, P. Y. Lee, C. C. Lin and Y. J. Chen, *Anal. Chem.*, 2008, **80**, 6159–6167.
32 S. A. Gomez-Lopera, J. L. Arias, V. Gallardo and A. V. Delgado, *Langmuir*, 2006, **22**, 2816–2821.
33 J. d. Vicente, A. V. Delgado, R. C. Plaza, J. D. G. Duran and F. Gonzales-Caballero, *Langmuir*, 2000, **16**, 7954–7961.
34 R. P. Bagwe, L. R. Hilliard and W. Tan, *Langmuir*, 2006, **22**, 4357–4362.
35 M. Baalousha and J. R. Lead, *Nat. Nanotechnol.*, 2013, **8**, 308–309.
36 S. V. Jadhav, D. S. Nikam, S. S. Mali, C. K. Hong and S. H. Pawar, *New J. Chem.*, 2014, **38**, 3678.
37 F. Mahmoud and N. Rivera, *Curr. Oncol. Rep.*, 2002, **4**, 250.
38 H. Tsai, C. Hsu, I. Chiu and C. B. Fuh, *Anal. Chem.*, 2007, **79**, 8416–8419.
39 M. Polanski and N. L. Anderson, *Biomarker Insights*, 2006, **1**, 1–48.
40 M. B. Pepys and G. M. Hirschfield, *J. Clin. Invest.*, 2003, **111**, 1805.
41 L. F. Steel, M. G. Trotter, P. B. Nakajima, T. S. Mattu, G. Gonye and T. Block, *Mol. Cell. Proteomics*, 2003, **2**, 262–270.
42 N. Tang, P. Tornatore and S. R. Weinberger, *Mass Spectrom. Rev.*, 2004, **23**, 34–44.
43 P. Aggarwal, J. B. Hall, C. B. McLeland, M. A. Dobrovolskaia and S. E. McNeil, *Adv. Drug Delivery Rev.*, 2009, **61**, 428–437.
44 M. Safi, J. Courtois, M. Seigneuret, H. Conjeaud and J.-F. Berret, *Biomaterials*, 2011, **32**, 9353–9363.
45 H. Kato, A. Nakamura, K. Takahashi and S. Kinugasa, *Nanomaterials*, 2012, **2**, 15–30.
46 W. Wang, X. Ji, H. B. Na, M. Safi, A. Smith, G. Palui, J. M. Perez and H. Mattoussi, *Langmuir*, 2014, **30**, 6197–6208.
47 R. Fürth and A. D. Cowper, *Investigations on the Theory of the Brownian Movement*, Dover Publications, Inc., 1956.
48 P. A. Hassan, S. Rana and G. Verma, *Langmuir*, 2015, **31**, 3–12.
49 M. A. Wells, A. Abid, I. M. Kennedy and A. I. Barakat, *Nanotoxicology*, 2012, **6**, 837–846.

